

Research paper

Magnetic chimeras in voltage-driven nano-oscillators

Susana Contreras-Celada ^{a,*}, René G. Rojas ^a, Saliya Coulibaly ^b, Marcel G. Clerc ^c,
Alejandro O. Leon ^d

^a Instituto de Física, Pontificia Universidad Católica de Valparaíso, Casilla 4059, Chile

^b Université de Lille, CNRS, UMR 8523 - PhLAM - Physique des Lasers Atomes et Molécules, F-59000 Lille, France

^c Departamento de Física and Millennium Institute for Research in Optics, Facultad de Ciencias Físicas y Matemáticas, Universidad de Chile, Casilla 487-3, Santiago, Chile

^d Departamento de Física, Facultad de Ciencias Naturales, Matemática y del Medio Ambiente, Universidad Tecnológica Metropolitana, Las Palmeras 3360, Ñuñoa 780-0003, Santiago, Chile

ARTICLE INFO

Keywords:

Chimeras
Synchronization
Decoherence
Magnetization dynamics
Voltage-controlled magnetic anisotropy

ABSTRACT

The emergence of spatiotemporal coherence is ubiquitous in nature. Intriguingly, in systems with uniform energy injection and dissipation mechanisms, coherent regions can be neighboring zones with non-coherent (e.g., chaotic or quasi-periodic) motions, giving rise to the so-called *chimera states*. This article studies the chimeric self-organization of magnetic nano-oscillators coupled with dipolar fields under energy losses and injection. The chimera states arise from an alternating voltage that, in the presence of insulating barriers, modulates the magnetic anisotropy fields, an effect known as *voltage-controlled magnetic anisotropy*. This field allows the efficient manipulation of the magnetization because it can produce magnetic switching and resonances, among other dynamic responses, while avoiding the Joule heating. In the classical limit, magnetization dynamics are governed by the Landau–Lifshitz equation. We consider three setups composed of $N = \{4, 6, 10\}$ interacting oscillators, each one of them regarded as a macrospin that moves rigidly. Our main results are *Small magnetic chimeras*, *Weak magnetic chimeras*, and a *meta-chaos* state. Chimera states are composed of a synchronized and a chaotic group of oscillators, both sets typically having hundreds of units; on the other hand, small chimeras are composed of a few – usually around five – oscillators dividing into coherent and non-coherent regions. A weak chimera has two or more sets of coherently oscillating units, but the groups possess different frequencies. Finally, the meta-chaos state is a chaotic transient. Beyond the previous zoology, fully synchronized states are also present, as the bifurcation diagram reveals.

1. Introduction

Non-equilibrium systems exhibit numerous dynamical behaviors [1–4], such as synchronized oscillations [5], chaotic and spatiotemporally chaotic states, spatially periodic patterns, and localized structures [2,4]. Under certain conditions, systems with uniform parameters can self-organize in two or more regions, displaying different dynamics separated by domain walls [1–4]. An iconic example is the so-called *chimera* state [6,7], where a set of oscillators evolve coherently while another group moves non-coherently. In the literature, the labels *coherent* and *non-coherent* typically refer to frequency-synchronized and chaotic or quasi-periodic dynamics, respectively. The term chimera has been employed since 2004 in nonlinear sciences [7] in resemblance to the

* Corresponding author.

E-mail address: susana.contreras@pucv.cl (S. Contreras-Celada).

<https://doi.org/10.1016/j.cnsns.2024.108420>

Received 27 May 2024; Received in revised form 5 September 2024; Accepted 28 October 2024

Available online 6 November 2024

1007-5704/© 2024 Elsevier B.V. All rights reserved, including those for text and data mining, AI training, and similar technologies.

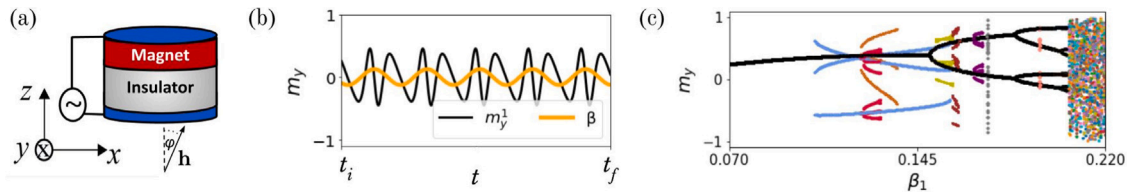


Fig. 1. Single VCMA-driven oscillator dynamics. (a) Schematic setup of a *magnetic metal/nonmagnetic insulator* bilayer, where an applied voltage increases or decreases the interfacial electron density. The magnetic field \mathbf{h} , tilted in φ radians from the z -axis, breaks the $m_z \rightarrow -m_z$ symmetry. (b) Trajectory of the m_y magnetization component (black curve) and the perpendicular-magnetic anisotropy function β (thicker yellowish curve) for $\beta_0 = 0.05$, $\omega = 0.08$, and $\beta_1 = 0.126$. Note that both functions oscillate with the same period T , i.e., $m_y(t) = m_y(t+T)$ and $\beta(t) = \beta(t+T)$. The initial and final times of the figure are $t_i = 92000$ and $t_f = 92400$. (c) Stroboscopic map of m_y as a function of the energy-injection parameter β_1 for several initial conditions. In this representation [49], for each β_1 value, and after a transient time, $m_y(t)$ is plotted every forcing period $T = 2\pi/\omega$. One can observe several oscillatory states and a period-doubling route to chaos. As in Ref. [49], the cycles are labeled by their period, e.g., a n -T state has an oscillation period equal to n times the forcing period. Then, the bifurcation diagram shows a 1-T (black) state and its period-doubling instabilities, leading to chaos. In addition, there are two 3-T states, one with a high (light blue) and one with a low (light brown) amplitude, a 9-T (crimson), 5-T (lemon green), 8-T (brown), 6-T (purple), and 16-T with a high (gray) and low (salmon) amplitude.

creature of Greek mythology composed of incongruous parts: a lion with a goat's and a snake's heads protruding from its back and tail. While the stabilization of the most common chimeras relies on a combination of bi-stability and nonlocal coupling [8,9], their existence in systems with local interactions has also been demonstrated [10,11]. Several chimeras emerge from hundreds of interacting oscillators; however, they also appear in smaller systems such as three pendulums [12], three-phase oscillators [13], and four lasers [14]. Those states are usually referred to as *small chimeras*. Another subclassification of chimeras includes the so-called *weak chimera* [15,16], where two regions possess internal frequency-synchronization, but the frequency is different from one zone to the other; *amplitude chimera* [17–21] showing the coexistence of regions with coherent and incoherent oscillation amplitude (rather than oscillation phase); and *freak chimera* [22], where the system exhibits two incoherent behaviors of different nature.

Ferromagnetic oscillators attract increasing attention due to their rich phenomenology, usually described in terms of their magnetization, and the possibility of using them as building blocks for information recording, processing, and transmission. Most of those applications rely on the bi- or multi-stability of magnetic systems and a switching mechanism that moves the magnetization from one stable equilibrium to another. Bi-stability is a signature of the nonlinear nature of hard magnets, and it arises from their magnetic anisotropy energies, which are usually quadratic in one of the magnetization components. The theoretical description of the magnetization evolution is based on the Landau–Lifshitz equation and its generalizations [23]. The solutions of this model, when the forcing is a (electric current-driven) magnetic field with a pulse- or sinusoidal-type time dependence, are magnetic switching and localized structures [24–26], among several others (see [23] and references therein). Beyond magnetic fields, spin-polarized charge currents [27] exert a torque to magnetic media that, depending on the current direction, enhances or counterbalances the magnetic dissipation, inducing self-oscillations [23,28,29], spatial textures [30–32], and chaos [33,34]. Even if spin-polarized currents can excite magnets in a much more localized region than magnetic fields, their power consumption is relatively high due to the Joule heating. Hence, the scientific quest for low-power-consumption forcing mechanisms for nano-scale magnetic devices is an active research field in the condensed matter community. One promising candidate is the *voltage-controlled magnetic anisotropy* (VCMA) effect, which allows modulation of the coefficient of the magnetic anisotropy energy by an external voltage. In the case of a *Magnetic metal/nonmagnetic insulator* bilayer, a transverse voltage generates a screening layer at the interface. Since all the magnetic properties of metals depend on the conduction-electron density, it is unsurprising that the voltage-induced density change modulates the perpendicular-anisotropy coefficient. The VCMA effect assists and induces magnetic switching [35,36], ferromagnetic resonance [37,38], and parametrically driven spin waves [39–43] and localized states [44]. Therefore, enhancing the VCMA's strength [45] and designing insulating magnets with VCMA capabilities [46,47] is a matter of current interest.

The VCMA-induced dissipative structures in single magnetic films with relatively large lateral dimensions have attracted substantial attention [35–45]. On the other hand, however, the dynamical responses induced by a VCMA field on several small interacting nano-oscillators remain mostly unknown and could have potential applications. For example, an oscillator array coupled with dipolar fields has been proposed as a reservoir computing structure [48]. Given that only one nano-oscillator under a time-periodic voltage exhibits a period-doubling route to chaos and vast regions of multi-stability in the parameter space [49], the dipolar coupling of several magnets may generate complexity. This article is devoted to predicting and characterizing the formation of *Small* and *Weak magnetic chimeras*, *fully synchronized states*, and *transient/meta chaos* in a set of VCMA-driven nano-oscillators. The system is described by the Landau–Lifshitz model and integrated numerically for several parameter values and initial conditions, as described in the next section.

2. Review of the single VCMA-driven nano-oscillator

Ferro- and ferrimagnetic materials are described by their magnetization vector $\mathbf{M} = M_s \mathbf{m}$, where the norm M_s is conserved at a fixed temperature, and \mathbf{m} is the unit magnetization. In the absence of chiral interactions, magnets of dimensions below ~ 100 nm exhibit uniform dynamics and evolve according to the dimensionless Landau–Lifshitz equation [23],

$$\dot{\mathbf{m}} = -\mathbf{m} \times \mathbf{h}_{\text{eff}} - \alpha \mathbf{m} \times (\mathbf{m} \times \mathbf{h}_{\text{eff}}), \quad (1)$$

where $\dot{\mathbf{m}}$ stands for the derivative of $\mathbf{m}(t)$ against the dimensionless time t , \mathbf{h}_{eff} is the effective magnetic field, and α is the phenomenological damping parameter. The first torque of Eq. (1) generates counter-clockwise rotations of \mathbf{m} around \mathbf{h}_{eff} . On the other hand, the term proportional to α in Eq. (1) dissipates the system energy. Then, the combination of both torques induces damped magnetization precessions that end when \mathbf{m} becomes parallel to \mathbf{h}_{eff} .

When the magnet is a thin film, \mathbf{h}_{eff} combines the external magnetic field $\mu_0 M_s \mathbf{h}$ and the perpendicular-magnetic anisotropy field $\mu_0 M_s \beta m_z \mathbf{e}_z$, with \mathbf{h} and $\beta m_z \mathbf{e}_z$ being their dimensionless counterparts, respectively. The symbol μ_0 stands for the magnetic permeability of free space and β the perpendicular-magnetic anisotropy coefficient. Let us consider the Cartesian representation shown in Fig. 1(a), where the plane $x - y$ is parallel to the magnet, and the z -axis is perpendicular to it. Using the Cartesian unit vectors $\{\mathbf{e}_x, \mathbf{e}_y, \mathbf{e}_z\}$ that point along the respective $\{x, y, z\}$ axes, the magnetization vector is decomposed as $\mathbf{m} = m_x \mathbf{e}_x + m_y \mathbf{e}_y + m_z \mathbf{e}_z$, with the norm constraint $\mathbf{m}^2 \equiv m_x^2 + m_y^2 + m_z^2 = 1$. The effective field is the \mathbf{m} -gradient of the magnetic energy E , and in its dimensionless form is

$$\mathbf{h}_{\text{eff}} = -\frac{\partial}{\partial \mathbf{m}} \left(\frac{E}{E_0} \right) = \mathbf{h} + \beta m_z \mathbf{e}_z, \quad (2)$$

where $E_0 = \mu_0 M_s^2 V_0$ is the energy scale of the magneto-dipolar interaction, V_0 is the volume, and the energy is

$$E = -E_0 \left(\mathbf{m} \cdot \mathbf{h} + \frac{\beta m_z^2}{2} \right). \quad (3)$$

It is worth noting that the energy of the perpendicular-magnetic anisotropy, $-E_0 \beta m_z^2 / 2$, is invariant against the $m_z \rightarrow -m_z$ transformation. Then, if $\mathbf{h} = 0$, the magnetization will have two equilibria with the same stability properties, namely, $\mathbf{m} = \pm \mathbf{e}_z$, *i.e.*, the magnetic film is a memory unit. The energy barrier to change the magnetic state depends on β . Indeed, for smaller β it is easier – and, then, energetically cheaper – to transit from one equilibrium to another. On the other hand, a large β favors the stability – and, therefore, the endurance – of the recorded state. Hence, the voltage-controlled magnetic anisotropy effect allows efficient dynamic control of β , interesting both from the technological viewpoint and the nonlinear dynamics perspective, particularly because β modulates the saturation mechanisms around magnetic equilibria.

Typically, the role of the external field \mathbf{h} is to rotate the magnetization towards a direction of interest, *e.g.*, to break the $m_z \rightarrow -m_z$ invariance. Since the β -dependent torque, $-\beta \mathbf{m} \times (m_z \mathbf{e}_z)$, vanishes if the magnetization points along the z -axis due to the cross product, then it is convenient to tilt the external field by an angle φ (in radians) from the vertical axis, *i.e.*,

$$\mathbf{h} = h [\cos(\varphi) \mathbf{e}_z + \sin(\varphi) \mathbf{e}_x]. \quad (4)$$

On the other hand, an alternating voltage produces a sinusoidal contribution to the anisotropy coefficient, $\beta(t) = \beta_0 + \beta_1 \cos(\omega t)$, where ω is the forcing angular frequency and β_1 is proportional to the applied voltage (see [46] and references therein). Fig. 1(b) shows a typical trajectory of the magnetization component $m_y(t)$ and $\beta(t)$. Both functions have the same oscillation period $T = 2\pi/\omega$. When the injection of energy is small, any initial condition reaches this periodic solution after transients, obeying $\mathbf{m}(t+T) = \mathbf{m}(t)$. This cycle appears as a single point for each β_1 value in the stroboscopic map, cf. Fig. 1(c). Note that for larger alternating voltages, β_1 , the solution suffers a series of bifurcations that double its period, satisfying $\mathbf{m}(t+2^n T) = \mathbf{m}(t)$ for an integer n . This cascade continues until reaching a chaotic state [49], as accounted by a positive largest Lyapunov exponent (LLE). A positive LLE demonstrates that initially close trajectories exponentially separate in the phase space. The bifurcation diagram, Fig. 1(c), also reveals the coexistence of other stable periodic solutions. The multi-stability of this single-oscillator system hints at the presence of complex solutions when several of these magnets interact, which is confirmed in the next section.

3. Coupled VCMA-forced nano-oscillators

3.1. Magnetization equations for coupled oscillators

Let us consider a linear array of magnetic oscillators with a first-neighbor spacing d , as shown in Fig. 2(a). The oscillators are equal, and they are subject to identical magnetic field and voltage, *i.e.*, the parameters M_s , V_0 , α , \mathbf{h} , β_0 , β_1 , and ω are the same. The dipolar energy between two small magnetic momenta $\boldsymbol{\mu}_i$ at \mathbf{r}_i and $\boldsymbol{\mu}_j$ at \mathbf{r}_j reads

$$E_{ij}^{(\text{dip})} = \frac{\mu_0}{4\pi} \frac{r_{ij}^2 \boldsymbol{\mu}_i \cdot \boldsymbol{\mu}_j - 3(\boldsymbol{\mu}_i \cdot \mathbf{r}_{ij})(\boldsymbol{\mu}_j \cdot \mathbf{r}_{ij})}{r_{ij}^5}, \quad (5)$$

where $\mathbf{r}_{ij} = r_{ij} \hat{\mathbf{r}}_{ij} \equiv \mathbf{r}_j - \mathbf{r}_i$ and $\boldsymbol{\mu}_i = M_s V_0 \mathbf{m}_i$. The dimensionless dipolar field exerted by \mathbf{m}_j on \mathbf{m}_i is

$$\mathbf{h}_{ij}^{(\text{dip})} = -\frac{\partial E_{ij}^{(\text{dip})}}{\partial (E_0 \mathbf{m}_i)} = \frac{V_0}{4\pi r_{ij}^3} [3\hat{\mathbf{r}}_{ij} (\mathbf{m}_j \cdot \hat{\mathbf{r}}_{ij}) - \mathbf{m}_j], \quad (6)$$

which is added to the Landau–Lifshitz equation of each i th oscillator,

$$\dot{\mathbf{m}}_i = -\mathbf{m}_i \times \left(\mathbf{h} + \beta m_{z,i} \mathbf{e}_z + \sum_{j \neq i} \mathbf{h}_{ij}^{(\text{dip})} \right) - \alpha \mathbf{m}_i \times \left[\mathbf{m}_i \times \left(\mathbf{h} + \beta m_{z,i} \mathbf{e}_z + \sum_{j \neq i} \mathbf{h}_{ij}^{(\text{dip})} \right) \right], \quad (7)$$

Note that this type of coupling is non-local because dipolar fields are long-range, *i.e.*, they decay as r^{-3} with distance r and then they reach beyond a few neighbors.

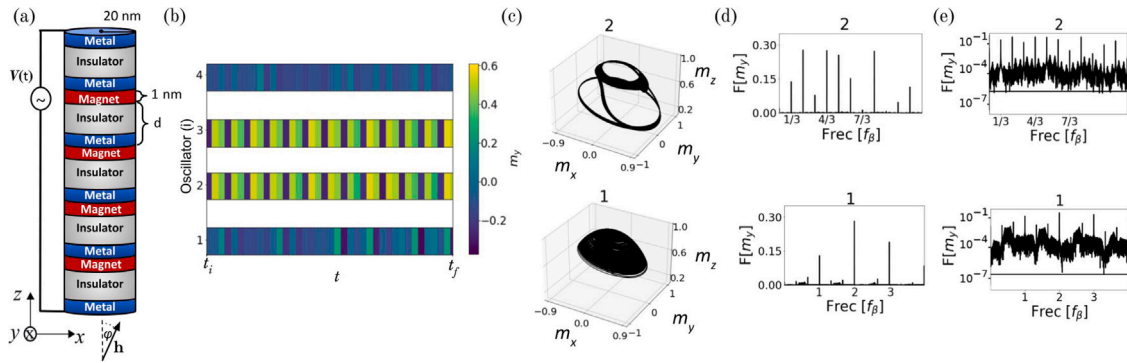


Fig. 2. *Small Magnetic Chimera* in a set of $N = 4$ VCMA-driven interacting oscillators. (a) Schematic representation of the setup of a system of four magnets. The dipolar fields couple the magnetizations with a strength that decays as d^{-3} . (b) Color map of the $m_{y,i}$ magnetization component plotted every forcing period T for the i th oscillator for $\beta_1 = 0.16$. The initial and final times are $t_i = 835620$ and $t_f = 838620$. The vertical axis labels the oscillator number (i), and a blank space is left between them for illustrative purposes. This kind of map allows identifying periodic motions, such as the one displayed by oscillators $i = 2$ and $i = 3$, which have period $3T$, and the aperiodic dynamics of 1st and 4th oscillators. (c) and (d) show the three-dimensional parametric plot of the magnetization trajectories and the Fourier spectrum of their m_y components for oscillators numbers 1 and 2. The largest Lyapunov exponent is $\lambda_{LLE} = 2 \times 10^{-3}$.

3.2. Geometric configuration

Given that typical magnetization trajectories have a large m_z component, a linear arrangement of the oscillators along the z -axis may favor synchronization since their dipolar fields will approximately lie along the magnetization direction. Note also that, according to Fig. 2(a), each magnet is sandwiched by a nonmagnetic metal and a nonmagnetic insulator, such as Cu and MgO. This configuration ensures that all magnets are subject to the same change in the interfacial charge density and, therefore, the $\beta(t)$ function is identical, β_1 becoming the control parameter associated with the energy injection of all oscillatory units. Motivated by Ref. [48], we consider a radius and a thickness of 20 nm and 1 nm, respectively, and then each magnetic volume is $V_0 = 1256.64 \text{ nm}^3$. In addition, let us consider $d = 50$ nm. Also, $r_{i,j} = d(j - i)$ and $\hat{\mathbf{r}}_{i,j} = \mathbf{e}_z$ for $j > i$. The interaction strength is ruled by the V_0/d^3 ratio. Note that Eq. (5) is only valid for very small magnets ($V_0/d^3 \ll 1$ limit), but it is still a good approximation that we may use for the sake of simplicity.

Note that given the small dimensions of this magnetic chain, all oscillators interact among them, which can be interpreted as a global type of coupling.

3.3. Numerical methods and dynamical indicators

For N interacting oscillators, we numerically integrate the corresponding N Landau–Lifshitz (vector) Eqs. (7), using a 4th-order Runge–Kutta algorithm [50] with a fixed step size $\Delta t = T/1000 = 0.0785$ for $\omega = 0.08$. Each Landau–Lifshitz equation is decomposed in the Cartesian representation, and the $|\mathbf{m}_i| = 1$ constraint is monitored through the temporal integration. The other parameters are $\alpha = 0.005$, $h = 0.1$, $\varphi = 0.3$, and $\beta_0 = 0.05$. The evolution is recorded from the end of the transient temporal interval $0 \leq t \leq 6 \times 10^5$, and the total integration time is $18000T = 1.4 \times 10^6$.

While several states with complicated trajectories are expected to emerge in this system of N oscillators, the characterization of their largest Lyapunov exponent (LLE) allows us to differentiate them as chaotic or non-chaotic. The LLE was calculated by characterizing the difference between two initial close trajectories, $\delta \vec{m}$, in the extended space of $3N$ Cartesian variables with N constraints from the norm conservation. In this notation $\delta \vec{m}^T = (\delta \mathbf{m}_1, \delta \mathbf{m}_2, \dots, \delta \mathbf{m}_N)^T$ and A^T stands for the transpose of A . The trajectory difference $\delta \vec{m}$ is small, i.e., $\|\delta \vec{m}\| \ll 1$, where $\|\vec{m}\|$ is the euclidean norm of the vector $\vec{m} \in \mathbb{R}^{3N}$ and it evolves according to the linear equation, $\delta \dot{\vec{m}} = \mathbb{J}(\mathbf{m}; t) \cdot \delta \vec{m}$, \mathbb{J} being the Jacobian. To account for the norm conservation, for each oscillator, the deviation function is normal to the magnetization, $\delta \mathbf{m}_i \cdot \mathbf{m}_i = 0$, i.e., the deviations lie in the (locally defined) tangent space of each spherical surface. Then, the largest Lyapunov exponent is given by

$$\lambda_{LLE} = \lim_{t \rightarrow \infty} \lim_{A_0 \rightarrow 0} \frac{1}{t} \ln \left[\frac{\|\delta \vec{m}(t)\|}{A_0} \right], \quad (8)$$

where $A_0 \equiv \|\delta \vec{m}(0)\|$ is the initial distance between the nearby trajectories in the phase space.

3.4. Small magnetic chimeras

Fig. 2 summarizes the typical dynamics observed in a system of four interacting units [see the schematic setup in Fig. 2(a)]. Since the magnetic multilayer has $3 \times 4 = 12$ magnetization components, it is convenient to represent the $m_{y,i}(t)$ of each magnet i th using a color map. Fig. 2(b) shows the stroboscopic evolution of the $m_{y,i}(t)$ components plotted every forcing period T . The horizontal axis is the (dimensionless) time, and the vertical axis is the oscillator label i . In the vertical axis, an empty space between

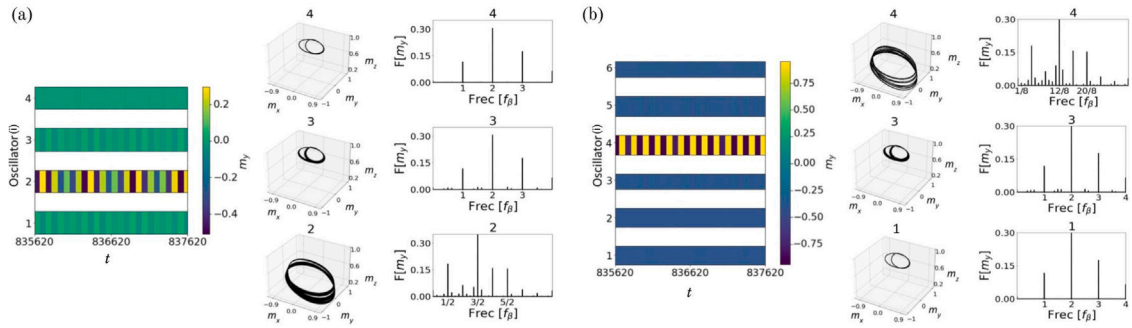


Fig. 3. *Weak Magnetic Chimeras* for a set of four and six coupled oscillators. The color maps, three-dimensional trajectories, and Fourier spectra are the same type of representation used in Fig. 2. (a) System of $N = 4$ oscillators, where $i = 2$ is desynchronized from the rest by displaying a quasi-periodic motion, the $i = 1, 3, 4$ units have a period T . (b) For $N = 6$, the 4th unit exhibits (an almost) close orbit of period $8T$, while the others have a period- T motion. For the states of (a) and (b), $\beta_1 = 0.126$, and the largest Lyapunov exponent is very small, i.e., $|\lambda_{\text{LLE}}| \sim 10^{-5}$, and falls within the numerical error.

the color sequences is left to illustrate that magnets are not in contact, but they interact via their long-range dipolar fields. As this graph reveals, there are two oscillators with an almost periodic motion and two others being aperiodic. The second ($i = 2$) and the third ($i = 3$) oscillators repeat their trajectories after three forcing periods, as seen from the color pattern. However, the aperiodic dynamics of the first ($i = 1$) and fourth ($i = 4$) oscillators affects the periodic motion of $\mathbf{m}_2(t)$ and $\mathbf{m}_3(t)$ via the dipolar fields. This perturbation is illustrated in Fig. 2(c) for the three-dimensional trajectories $\mathbf{m}_2(t)$ and $\mathbf{m}_3(t)$. Therefore, while strictly speaking, the whole system is aperiodic due to the global (dipolar) coupling, we shall call the slightly disturbed periodic dynamics simple as *periodic* in the rest of this document, e.g., $i = 2$ and $i = 3$ will be referred to as periodic, or coherence, units. On the other hand, the $i = 1$ and $i = 4$ oscillators exhibit a complex dynamics, as exemplified in Fig. 2(c) by the $\mathbf{m}_1(t)$ trajectory that almost fill the upper region of unit spherical surface. Indeed, the largest Lyapunov exponent is $\lambda_{\text{LLE}} = 2 \times 10^{-3}$, showing the chaotic character of this incoherent unit. This implies that, the 1st and 4th oscillators have an exponential sensibility to the initial conditions. Another useful representation is the Fourier spectrum of the temporal series $m_{y,i}(t)$. In the case of the periodic magnets, there is a clear set of peaks with the fundamental frequency $f = f_\beta/3$, where the forcing frequency is $f_\beta = \omega/(2\pi)$, c.f., Fig. 2(d). The small noise-like disturbances to this spectrum are attributed to the aperiodic dipolar fields generated by $\mathbf{m}_1(t)$ and $\mathbf{m}_4(t)$. Since this state combines a coherent and non-coherent behavior, it corresponds to a *Small Magnetic Chimera*.

3.5. Weak magnetic chimeras

Another example of chimeric behavior is shown in Fig. 3(a) and Fig. 3(b) for systems of $N = 4$ and $N = 6$ units, respectively. In this case, one periodic magnetization is embedded in a set of other periodic oscillators with a different frequency, resulting in a quasi-periodic motion for the whole system. Indeed, as Fig. 3(a) illustrates, the $i = 1, 3, 4$ oscillators have three dominant frequencies that are equal to one, two, and three times the forcing frequency. However, the $i = 2$ unit has a clean Fourier spectrum with a large peak at half of the forcing frequency (and its harmonics). Regarding this single oscillator as a small region, and following Refs. [15,16], we refer to this state as a *Weak Magnetic Chimera*, to emphasize that this dissipative structure is composed of two regions displaying different coherent states. In Fig. 3(a), the $i = 2$ oscillators exhibit a limit cycle with a large Fourier peak at $f_\beta/2$, while the $i = 1, 3, 4$ units have a fundamental frequency equal to f_β . It is worth noting that the fourth unit, which is farther apart from the second oscillator, has a well-defined closed orbit in the three-dimensional plot of $\mathbf{m}_4(t)$, which corresponds to a clean Fourier spectrum. On the other hand, the three-dimensional trajectories and Fourier spectra of $i = 2$ and $i = 3$ reveal their interaction effects by dipolar fields, i.e., they introduce their frequency by dipolar fields, generating additional Fourier peaks. In a similar way, in the system of $N = 6$ oscillators, the 4th unit has a period of $8T$, different from the T period of the rest of the magnets. Indeed, for $i = 1, 2, 3, 5, 6$, the color map shows an almost constant texture, as expected from a stroboscopic map that plots the $m_{y,i}(t + nT)$ with n an integer. Comparing the Fourier spectrum of $i = 1$ and $i = 3$ we can see that small additional peaks are introduced in the surroundings of $i = 4$, but decay fast with the distance r as expected from the r^{-3} scaling of the dipolar interaction. Since the oscillators are periodic, except for the small response to the dipolar field of the desynchronized unit, their LLE is negative. The non-zero largest Lyapunov exponent of the cycle originates from the locking oscillation phase, i.e., the magnetizations lock their oscillation phase due to the a.c. voltage.

3.6. Fully synchronized states and meta-chaos

Finally, a general third kind of dynamics observed in this system corresponds to a *Fully Synchronized State*, as shown in Fig. 4(b). In this state, all units have the same oscillation frequency and phase. Furthermore, when the system is integrated from a set of randomly chosen initial conditions, the most commonly observed attractor is totally synchronized. However, in the particular case of Fig. 4, the system exhibits chaotic dynamics for a long time before converging to the synchronized state; that is, it shows a

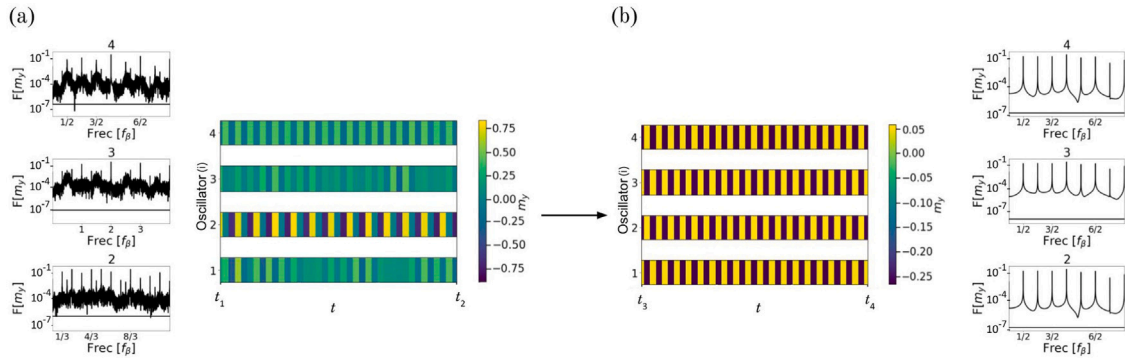


Fig. 4. Meta-chaos (also known as transient chaos) for a system of $N = 4$ units. The Fourier spectrum and color-map representations are the same of the previous figures. The left panel, (a), shows the dynamics in a chaotic regime characterized by a positive LLE, $\lambda_{LLE} = 2 \times 10^{-3}$. This state is not a chimera because there is no coherent region. Indeed, $i = 1$ and $i = 3$ are aperiodic and $i = 2$ and $i = 4$ display nearly periodic motions with period $3T$ and $2T$, respectively. However, if the transient time is incremented by a factor 10, the system fully synchronizes into an orbit with period $2T$, as revealed in (b), where $\lambda_{LLE} = -5 \times 10^{-4}$. The time limits of the graph are $t_1 = 835620$, $t_2 = 838620$, $t_3 = 14005620$, and $t_4 = 14008620$, and $\beta_1 = 0.16$.

meta (or transient) chaos [51]. Therefore, $\lambda_{LLE} = 2 \times 10^{-3}$ if the Lyapunov exponent is calculated in a large enough time window. However, if the system integration time is about 10 times larger, the fully synchronized state has a $\lambda_{LLE} = -5 \times 10^{-4}$, as expected. In Fig. 4, the Fourier spectra at the left and right are noisy and clean, respectively, as characteristic spectra of chaotic and periodic attractors.

3.7. Bifurcation diagram

Fig. 5 summarizes the dynamics of $N = 10$ oscillators and compares them with results for systems with $N = 4$ and $N = 6$ in the bifurcation diagram of Fig. 5(a). This phase diagram was obtained by integrating 100 randomly chosen initial conditions and analyzing the resulting dynamics after the transient time of $12000(2\pi/\omega)$. For each one of the 100 initial conditions, the classification of each state was conducted via the visual inspection of the colormaps, parametric plots, and Fourier spectra. As this figure reveals, the most robust state is a fully synchronized magnetization motion where all units have the same frequency. This state is present for all N and β_1 values, except for $\beta_1 = 0.13$. Is it worth noting that weak magnetic chimeras are also robust. Fig. 5(b) shows a small magnetic chimera state, where the $i = 2, 3, 4, 7, 8, 9$ units are synchronized in periodic oscillations ($3T$), while the units $i = 1, 5, 6, 10$ are chaotic. Similar to the $N = 4$ and $N = 6$ systems, the periodic oscillators are perturbed by the chaotic ones. On the other hand, Fig. 5(c) shows a frequency-synchronized state with a frequency $f = (2T)^{-1}$. Finally, Fig. 5(d) reveals a weak magnetic chimera number of oscillators ($i = 1, 2, 3, 4, 9, 10$) with periodic motion of period $2T$, while $i = 5, 6, 7, 8$ have period $3T$.

3.8. Localization of the complexity

To deepen the discussion on the system complexity, let us stress that for a chaotic state, the initially small separation of trajectories amplifies with time, i.e., the solution of the Jacobian equation reads

$$\delta\vec{m}(t) \approx \delta\vec{m}_0 e^{\lambda_{LLE}t}, \tag{9}$$

$$\delta\vec{m}_0^T = (\delta\mathbf{m}_{1,0}, \delta\mathbf{m}_{2,0}, \dots, \delta\mathbf{m}_{N,0})^T, \tag{10}$$

where $\delta\vec{m}_0$ is a characteristic function of time and $e^{\lambda_{LLE}t}$ accounts for the exponential growth (for $\lambda_{LLE} > 0$) or decay (for $\lambda_{LLE} < 0$). The case $\lambda_{LLE} = 0$ usually corresponds to a cycle where the phase is a neutral mode. Non-exponential, such as polynomial, growth, and decay, are also characterized by a zero LLE. In our system, however, the magnetic oscillators attempt to synchronize with the external magnetic field, fixing both their frequency and phase. This breaking of the oscillation-phase invariance results in periodic motions with $\lambda_{LLE} < 0$. The general solution of the Jacobian equation is expanded in a set of eigenfunctions, whose corresponding eigenvalues are referred to as the Lyapunov spectrum. However, since the largest Lyapunov exponent is the maximum value of this spectrum, the $e^{\lambda_{LLE}t}$ function dominates the general solution for $\delta\vec{m}(t)$.

Let us concentrate on a chaotic state. The growth of $\delta\vec{m}(t)$ is not uniformly distributed in the $3N$ space, but it depends on the relative size of the $\delta\mathbf{m}_{i,0}$ functions, implying that the system can be more sensitive to the initial conditions in some oscillators than in others, which depends on the $|\delta\mathbf{m}_{i,0}|$, as accounted by

$$\|\delta\vec{m}_0\|^2 = \sum_{i=1}^N |\delta\mathbf{m}_{i,0}|^2. \tag{11}$$

Then, if the temporal average of $|\delta\mathbf{m}_{i,0}|$ is larger than the one of $|\delta\mathbf{m}_{j,0}|$, it implies that the exponential sensibility of the system to the initial conditions of the i th oscillator is larger than the one of the j th unit. The same analysis is conducted for $\lambda_{LLE} < 0$, where

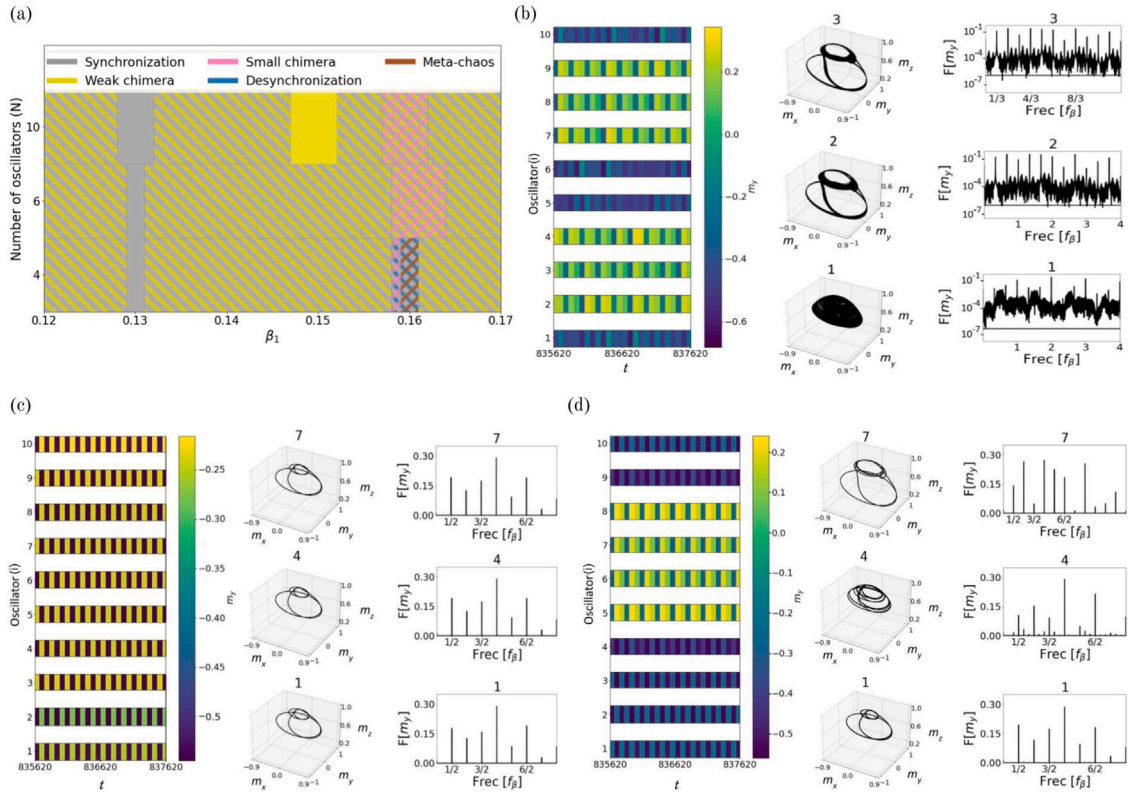


Fig. 5. Phenomenology of an $N = 10$ system and its comparison with the dynamics for $N = 4$ and $N = 6$. (a) Bifurcation diagram of the system. The Fully Synchronized State, Small and Weak Magnetic Chimeras, Meta-Chaos, and a Desynchronized State are shown as a function of the number of oscillators and the energy injection parameter, β_1 . This plot was obtained by integrating 300 randomly chosen initial conditions for each N and β_1 . The horizontal step size is $\Delta\beta_1 = 0.01$ (b) Small magnetic chimera, where the oscillators $i = 2, 3, 4, 7, 8, 9$ have periodic motion with period $3T$, while the 1st, 5th, 6th, and 10th units are chaotic. (c) Fully synchronized state of period $2T$. (d) Weak magnetic chimera, where the magnets $i = 5, 6, 7, 8$ have an oscillation period of $3T$, and the rest have a period of $2T$. Here, $\beta_1 = 0.16$, and the LLE for (b), (c), and (d) are 2×10^{-3} , -5×10^{-5} and -5×10^{-5} , respectively.

the oscillators with a larger $|\delta\mathbf{m}_{i,0}|$ have a larger convergence time, *i.e.*, need more time to reach the attractor fully. For the case of $N = 10$ oscillators, Fig. 6 shows the temporal average $|\delta\mathbf{m}^i| \equiv \tau^{-1} \int_{t_0}^{t_0+\tau} dt |\delta\mathbf{m}_{i,0}|$ demonstrating that the complexity localizes around the desynchronized units, particular, around the incoherent oscillators for the Small chimeras.

4. Conclusions

While coherent and non-coherent states are ubiquitous in nature and have been vastly studied in the last decades, their chimeric coexistence has received less attention. This article studied Magnetic Chimeras in a linear array of magnetic oscillators driven by a time-dependent voltage. The structure has insulating barriers that prevent the formation of a charge current. Then, the effect of the voltage is to create screening charges at the system interfaces, which in turn modulate the magnetic anisotropies. This effect is known as *voltage-controlled magnetic anisotropies*, and it has the capacity to induce magnetization dynamics without the undesirable Joule heating, becoming a promising candidate for applications to memory technologies. Each magnet is described by the Landau–Lifshitz equation within the macrospin approximation, that is, assuming that the magnetic materials are small enough to ensure the rigid motion of their magnetizations and that they interact by their dipolar fields. Therefore, the system under study is a set of globally coupled magnets subject to a periodic injection of energy. Integrating the set of coupled Landau–Lifshitz equations numerically, we found that the voltage induces *Fully Synchronized States* where all units oscillate with the same frequency and phase. In addition, we report *Weak Magnetic Chimeras* where one or a few periodic units are embedded in a periodic background of oscillators. The system also exhibits *Small Magnetic Chimeras*, where domains of coherent (periodic) and non-coherent (chaotic) motions exist. Finally, a *Chaotic Transient (Meta-Chaos)* was observed. Using the largest Lyapunov exponent (LLE), we could characterize the complexity of the system. The eigenfunction of the LLE shows a clear localization around the magnet whose motion is aperiodic, confirming that this oscillatory unit is particularly sensitive to the initial conditions. The bifurcation diagram of the system reveals that the Fully Synchronized State and Weak Magnetic Chimeras are much more robust than the Small Magnetic Chimeras and Meta-Chaos.

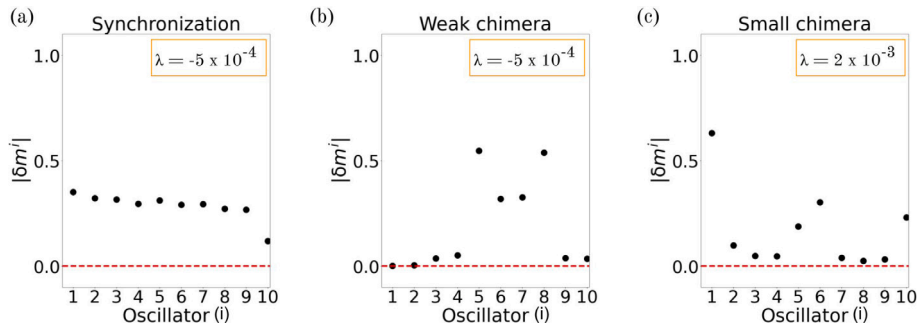


Fig. 6. Spatial localization of the complexity for a system of $N = 10$ oscillators. The difference between two initially close trajectories is an exponential function, $\delta\vec{m}(t) \approx \delta\vec{m}_0 e^{\lambda_{LLE} t}$. Note that $\delta\vec{m}(t)$ is not uniformly distributed in the $3N$ space, but it localizes more on some oscillators, as accounted by the relative size of the $|\delta\vec{m}_{i,0}|$ norms. In this figure, the temporal average $|\delta\vec{m}'| \equiv \tau^{-1} \int_{t_0}^{t_0+\tau} dt |\delta\vec{m}_{i,0}|$. Indeed, if $\lambda_{LLE} > 0$, a larger $|\delta\vec{m}'|$ implies that the i th magnet is more sensitive to its initial conditions. (a) For a fully synchronized state, $\lambda_{LLE} = 0$, and the convergence of the oscillators is similar. (b) Weak magnetic chimeras are non-chaotic and, for this case, $\lambda_{LLE} = 0$. As this plot illustrates, the $i = 5, 6, 7, 8$ have a larger $|\delta\vec{m}'|$ since they are the desynchronized oscillators. (c) The Small magnetic chimera has $\lambda_{LLE} > 0$, and the $|\delta\vec{m}'|$ is much larger, implying that the chaos (sensitivity to the initial conditions) localized mostly around this unit. For this figure, $\beta_1 = 0.16$.

CRedit authorship contribution statement

Susana Contreras-Celada: Writing – review & editing, Software, Investigation, Conceptualization. **René G. Rojas:** Writing – review & editing, Supervision, Conceptualization. **Saliya Coulibaly:** Validation, Supervision, Methodology, Funding acquisition. **Marcel G. Clerc:** Supervision, Methodology, Conceptualization. **Alejandro O. Leon:** Writing – original draft, Supervision, Funding acquisition, Conceptualization.

Declaration of competing interest

The authors declare that they have no known competing financial interests or personal relationships that could have appeared to influence the work reported in this paper.

Acknowledgments

We gratefully acknowledge financial support in Chile from FONDECYT Grant 11230120, 1210353, and 3190030. SC-C, RJ, and AL gratefully thank the PROGRAMA DE COOPERACION CIENTIFICA ECOS-ANID ECOS200006. SC acknowledges support from the program ECOS-Sud C20E07. MC thanks ANID-Millennium Science Initiative Program- ICN17-012 (MIRO). This research was supported by the Cluster Faraday UTEM (CONICYT- FONDEQUIP – EQM180180).

Data availability

Data will be made available on request.

References

- [1] Nicolis G, Prigogine I. Self-organization in nonequilibrium systems. New York: J. Wiley & Sons; 1977. <http://dx.doi.org/10.1002/bbpc.197800155>.
- [2] Cross MC, Hohenberg PC. Pattern formation outside of equilibrium. Rev Modern Phys 1993;65:851. <http://dx.doi.org/10.1103/RevModPhys.65.851>.
- [3] Scott A. Encyclopedia of nonlinear science. Routledge; 2006. <http://dx.doi.org/10.4324/9780203647417>.
- [4] Pismen L. Patterns and interfaces in dissipative dynamics. Springer; 2006. http://dx.doi.org/10.1007/978-0-387-30440-3_381.
- [5] Pikovsky A, Rosenblum M, Kurths J. Synchronization: a universal concept in nonlinear sciences. Cambridge University Press; 2001. <http://dx.doi.org/10.1017/CBO9780511755743>.
- [6] Kuramoto Y, Battogtokh D. Coexistence of coherence and incoherence in nonlocally coupled phase oscillators. Nonlinear Phenom Complex Syst 2002;5:380.
- [7] Abrams DM, Strogatz SH. Chimera states for coupled oscillators. Phys Rev Lett 2004;93:174102. <http://dx.doi.org/10.1103/PhysRevLett.93.174102>.
- [8] Sethia GC, Sen A. Chimera states: The existence criteria revisited. Phys Rev Lett 2014;112:144101. <http://dx.doi.org/10.1103/PhysRevLett.112.144101>.
- [9] Yeldesbay A, Pikovsky A, Rosenblum M. Chimeralike states in an ensemble of globally coupled oscillators. Phys Rev Lett 2014;112:144103. <http://dx.doi.org/10.1103/PhysRevLett.112.144103>.
- [10] Laing CR. Chimeras in networks with purely local coupling. Phys Rev E 2015;92:050904. <http://dx.doi.org/10.1103/PhysRevE.92.050904>, <https://link.aps.org/doi/10.1103/PhysRevE.92.050904>.
- [11] Clerc MG, Coulibaly S, Ferré MA, García-Núñez MA, Rojas RG. Chimera-type states induced by local coupling. Phys Rev E 2016;93:052204. <http://dx.doi.org/10.1103/PhysRevE.93.052204>, <https://link.aps.org/doi/10.1103/PhysRevE.93.052204>.
- [12] Wojewoda J, Czołczyński K, Maistrenko Y, Kapitaniak T. The smallest chimera state for coupled pendula. Sci Rep 2016;6:34329. <http://dx.doi.org/10.1038/srep34329>.

- [13] Maistrenko Y, Brezetsky S, Jaros P, Levchenko R, Kapitaniak T. Smallest chimera states. *Phys Rev E* 2017;95:010203. <http://dx.doi.org/10.1103/PhysRevE.95.010203>.
- [14] Röhm A, Böhm F, Lüdge K. Small chimera states without multistability in a globally delay-coupled network of four lasers. *Phys Rev E* 2016;94:042204. <http://dx.doi.org/10.1103/PhysRevE.94.042204>, <https://link.aps.org/doi/10.1103/PhysRevE.94.042204>.
- [15] Ashwin P, Burylko O. Weak chimeras in minimal networks of coupled phase oscillators. *Chaos* 2015;25:013106. <http://dx.doi.org/10.1063/1.4905197>.
- [16] Manoj K, Pawar SA, Dange S, Mondal S, Sujith RI, Surovyatkina E, et al. Synchronization route to weak chimera in four candle-flame oscillators. *Phys Rev E* 2019;100:062204. <http://dx.doi.org/10.1103/PhysRevE.100.062204>.
- [17] Zakharova A, Kapeller M, Schöll E. Chimera death: Symmetry breaking in dynamical networks. *Phys Rev Lett* 2014;112:154101. <http://dx.doi.org/10.1103/PhysRevLett.112.154101>.
- [18] Banerjee T. Mean-field-diffusion-induced chimera death state. *Europhys Lett* 2015;110:60003. <http://dx.doi.org/10.1209/0295-5075/110/60003>.
- [19] Banerjee T, Dutta PS, Zakharova A, Schöll E. Chimera patterns induced by distance-dependent power-law coupling in ecological networks. *Phys Rev E* 2016;94:032206. <http://dx.doi.org/10.1103/PhysRevE.94.032206>.
- [20] Cano AV, Cosenza MG. Asymmetric cluster and chimera dynamics in globally coupled systems. *Chaos* 2018;28:113119. <http://dx.doi.org/10.1063/1.5043398>.
- [21] Clerc MG, Coulibaly S, Ferre MA, Rojas RG. Chimera states in a duffing oscillator chain coupled to nearest neighbors. *Chaos* 2018;28:083126. <http://dx.doi.org/10.1063/1.5025038>.
- [22] Clerc MG, Coulibaly S, Ferre MA. Freak chimera states in a locally coupled Duffing oscillators chain. *Commun Nonlinear Sci Numer Simul* 2020;89:105288. <http://dx.doi.org/10.1016/j.cnsns.2020.105288>.
- [23] Mayergoyz ID, Bertotti G, Serpico C. *Nonlinear magnetization dynamics in nanosystems*. Oxford: Elsevier; 2009. <http://dx.doi.org/10.1016/B978-0-08-044316-4.X0001-1>.
- [24] Mikeska HJ. Solitons in a one-dimensional magnet with an easy plane. *J Phys C* 1978;11:L29. <http://dx.doi.org/10.1088/0022-3719/11/1/007>.
- [25] Clerc MG, Coulibaly S, Laroze D. Localized waves in a parametrically driven magnetic nanowire. *Europhys Lett* 2012;97:30006. <http://dx.doi.org/10.1209/0295-5075/97/30006>.
- [26] Berrios-Caro E, Clerc MG, Leon AO. Flaming 2π kinks in parametrically driven systems. *Phys Rev E* 2016;94:052217. <http://dx.doi.org/10.1103/PhysRevE.94.052217>.
- [27] Ralph DC, Stiles MD. Spin transfer torques. *J Magn Magn Mater* 2008;320:1190. <http://dx.doi.org/10.1016/j.jmmm.2007.12.019>.
- [28] Kiselev SI, Sankey JC, Krivorotov IN, Emlay NC, Schoelkopf RJ, Buhrman RA, et al. Microwave oscillations of a nanomagnet driven by a spin-polarized current. *Nature* 2003;425:380. <http://dx.doi.org/10.1038/nature01967>.
- [29] Slavin A, Tiberkevich V. Nonlinear auto-oscillator theory of microwave generation by spin-polarized current. *IEEE Trans Magn* 2009;45:1875. <http://dx.doi.org/10.1109/TMAG.2008.20099357>.
- [30] Volkov OM, Kravchuk VP, Sheka DD, Mertens FG, Gaididei Y. Periodic magnetic structures generated by spin polarized currents in nanostripes. *Appl Phys Lett* 2013;103:222401. <http://dx.doi.org/10.1063/1.4831748>.
- [31] Kravchuk VP, Volkov OM, Sheka DD, Gaididei Y. Periodic magnetization structures generated by transverse spin current in magnetic nanowires. *Phys Rev B* 2013;87:224402. <http://dx.doi.org/10.1103/PhysRevB.87.224402>.
- [32] Leon AO, Clerc MG. Spin-transfer-driven nano-oscillators are equivalent to parametric resonators. *Phys Rev B* 2015;91:014411. <http://dx.doi.org/10.1103/PhysRevB.91.014411>.
- [33] Berkov D, Gorn N. Transition from the macrospin to chaotic behavior by a spin-torque driven magnetization precession of a square nanoelement. *Phys Rev B* 2005;71:052403. <http://dx.doi.org/10.1103/PhysRevB.71.052403>.
- [34] Cabanas AM, Clerc MG, Laroze D, Leon AO. Chaotic patterns and localized states in spin valves. *J Magn Magn Mater* 2019;476:589. <http://dx.doi.org/10.1016/j.jmmm.2019.01.027>.
- [35] Shiota Y, Maruyama T, Nozaki T, Shinjo T, Shiraiishi M, Suzuki Y. Voltage-assisted magnetization switching in ultrathin Fe₈₀Co₂₀ alloy layers. *Appl Phys Express* 2009;2:063001. <http://dx.doi.org/10.1143/APEX.2.063001>.
- [36] Kanai S, Yamanouchi M, Ikeda S, Nakatani Y, Matsukura F, Ohno H. Electric field-induced magnetization reversal in a perpendicular-anisotropy CoFeB-MgO magnetic tunnel junction. *Appl Phys Lett* 2012;101:122403. <http://dx.doi.org/10.1063/1.4753816>.
- [37] Nozaki T, Shiota Y, Miwa S, Murakami S, Bonell F, Ishibashi S, et al. Electric-field-induced ferromagnetic resonance excitation in an ultrathin ferromagnetic metal layer. *Nat Phys* 2012;8:491. <http://dx.doi.org/10.1038/nphys2298>.
- [38] Zhu J, Katine JA, Rowlands GE, Chen YJ, Duan Z, Alzate JG, et al. Voltage-induced ferromagnetic resonance in magnetic tunnel junctions. *Phys Rev Lett* 2012;108:197203. <http://dx.doi.org/10.1103/PhysRevLett.108.197203>.
- [39] Verba R, Carpentieri M, Finocchio G, Tiberkevich V, Slavin A. Amplification and stabilization of large-amplitude propagating spin waves by parametric pumping. *Appl Phys Lett* 2018;112:042402. <http://dx.doi.org/10.1063/1.5019357>.
- [40] Verba R, Tiberkevich V, Krivorotov IN, Slavin A. Parametric excitation of spin waves by voltage-controlled magnetic anisotropy. *Phys Rev Appl* 2014;1:044006. <http://dx.doi.org/10.1103/PhysRevApplied.1.044006>.
- [41] Verba R, Carpentieri M, Finocchio G, Tiberkevich V, Slavin A. Excitation of propagating spin waves in ferromagnetic nanowires by microwave voltage-controlled magnetic anisotropy. *Sci Rep* 2016;6:25018. <http://dx.doi.org/10.1038/srep25018>.
- [42] Rana B, Fukuma Y, Miura K, Takahashi H, Otani Y. Excitation of coherent propagating spin waves in ultrathin CoFeB film by voltage-controlled magnetic anisotropy. *Appl Phys Lett* 2017;111:052404. <http://dx.doi.org/10.1063/1.4990724>.
- [43] Taniguchi T. Non-periodic input-driven magnetization dynamics in voltage-controlled parametric oscillator. *J Magn Magn Mater* 2022;563:170009. <http://dx.doi.org/10.1016/j.jmmm.2022.170009>.
- [44] Leon AO, Clerc MG, Altibr D. Dissipative magnetic breathers induced by time-modulated voltages. *Phys Rev E* 2018;98:062213. <http://dx.doi.org/10.1103/PhysRevE.98.062213>.
- [45] Nozaki T, Yamamoto T, Miwa S, Tsujikawa M, Shirai M, Yuasa S, et al. Recent progress in the voltage-controlled magnetic anisotropy effect and the challenges faced in developing voltage-torque MRAM. *Micromachines* 2019;10:327. <http://dx.doi.org/10.3390/mi10050327>.
- [46] Leon AO, Cahaya AB, Bauer GEW. Voltage control of rare-earth magnetic moments at the magnetic-insulator metal interface. *Phys Rev Lett* 2018;120:027201. <http://dx.doi.org/10.1103/PhysRevLett.120.027201>.
- [47] Leon AO, Bauer GEW. Voltage- and temperature-dependent rare-earth dopant contribution to the interfacial magnetic anisotropy. *J Phys: Condens Matter* 2020;32:404004. <http://dx.doi.org/10.1088/1361-648x/ab997c>.
- [48] Nomura H, Furuta T, Tsujimoto K, Kuwabiraki Y, Peper F, Tamura E, et al. Reservoir computing with dipole-coupled nanomagnets. *Japan J Appl Phys* 2019;58:070901. <http://dx.doi.org/10.7567/1347-4065/ab2406>, <https://iopscience.iop.org/article/10.7567/1347-4065/ab2406>.
- [49] Contreras-Celada S, Clerc MG, Coulibaly S, Rojas RG, Leon AO. Voltage-driven multistability and chaos in magnetic films. *J Magn Magn Mater* 2022;562:169793. <http://dx.doi.org/10.1016/j.jmmm.2022.169793>.
- [50] Press WH, Teukolsky SA, Vetterling WT, Flannery BP. *Numerical recipes in c. Vol. 2*, Cambridge: Cambridge University Press; 1996.
- [51] Yorke JA, Yorke ED. Metastable chaos: The transition to sustained chaotic behavior in the Lorenz model. *J Stat Phys* 1979;21:263. <http://dx.doi.org/10.1007/BF01011469>, <https://link.springer.com/article/10.1007/BF01011469>.